



**HAL**  
open science

## Aperiodic quantum oscillations in the two-dimensional electron gas at the LaAlO<sub>3</sub>/SrTiO<sub>3</sub> interface

Km Rubi, Julien Gosteau, Raphaël Serra, Kun Han, Shengwei Zeng, Zhen Huang, Bénédicte Warot-Fonrose, Rémi Arras, Etienne Snoeck, Ariando Ariando, et al.

► **To cite this version:**

Km Rubi, Julien Gosteau, Raphaël Serra, Kun Han, Shengwei Zeng, et al.. Aperiodic quantum oscillations in the two-dimensional electron gas at the LaAlO<sub>3</sub>/SrTiO<sub>3</sub> interface. *Npj Quantum Materials*, 2020, 5, pp.9. 10.1038/s41535-020-0210-z . hal-02988958

**HAL Id: hal-02988958**

**<https://hal.science/hal-02988958v1>**

Submitted on 20 Nov 2020

**HAL** is a multi-disciplinary open access archive for the deposit and dissemination of scientific research documents, whether they are published or not. The documents may come from teaching and research institutions in France or abroad, or from public or private research centers.

L'archive ouverte pluridisciplinaire **HAL**, est destinée au dépôt et à la diffusion de documents scientifiques de niveau recherche, publiés ou non, émanant des établissements d'enseignement et de recherche français ou étrangers, des laboratoires publics ou privés.

## ARTICLE OPEN

Aperiodic quantum oscillations in the two-dimensional electron gas at the LaAlO<sub>3</sub>/SrTiO<sub>3</sub> interfaceKm Rubi<sup>1,4\*</sup>, Julien Gosteau<sup>2</sup>, Raphaël Serra<sup>2</sup>, Kun Han<sup>3</sup>, Shengwei Zeng<sup>3</sup>, Zhen Huang<sup>3</sup>, Benedicte Warot-Fonrose<sup>2</sup>, Rémi Arras<sup>2</sup>, Etienne Snoeck<sup>2</sup>, Ariando<sup>3\*</sup>, Michel Goiran<sup>1</sup> and Walter Escoffier<sup>1</sup>

Despite several attempts, the intimate electronic structure of two-dimensional electron systems buried at the interface between LaAlO<sub>3</sub> and SrTiO<sub>3</sub> still remains to be experimentally revealed. Here, we investigate the transport properties of a high-mobility quasi-two-dimensional electron gas at this interface under high magnetic field (55 T) and provide new insights for electronic band structure by analyzing the Shubnikov-de Haas oscillations. Interestingly, the quantum oscillations are not  $1/B$ -periodic and produce a highly non-linear Landau plot (Landau level index versus  $1/B$ ). We explore different scenarios leading to  $1/B$ -aperiodic oscillations where the charge and the chemical potential vary as the magnetic field increases. Overall, the magneto-transport data are discussed in light of high-resolution scanning transmission electron microscopy (HRSTEM) analysis of the interface as well as calculations from density functional theory.

npj Quantum Materials (2020)5:9; <https://doi.org/10.1038/s41535-020-0210-z>

## INTRODUCTION

The discovery of a two-dimensional electron gas (2DEG) at the interface between two insulators LaAlO<sub>3</sub> (LAO) and SrTiO<sub>3</sub> (STO)<sup>1</sup> has not only enhanced the expectations in oxide-electronics but has also brought new and exciting opportunities to explore the novel physics of 2DEG with unmapped parameters. In recent years, this interface has been studied extensively and several exotic phenomena including superconductivity,<sup>2–4</sup> Rashba spin-orbit coupling,<sup>5–7</sup> ferromagnetism,<sup>8–10</sup> and quantum oscillations<sup>11–14</sup> have been reported. The leading consensus for the formation of the 2DEG at this interface is the electronic reconstruction (also referred to as the “polar catastrophe”).<sup>15,16</sup> This scenario is based on electron transfer from the polar LAO to the interfacial layers of STO, although other mechanisms such as oxygen vacancy doping<sup>17,18</sup> or interdiffusion<sup>19</sup> are also at play.

First-principles calculations of the band-structure reveal the occupancy of several non-degenerate sub-bands  $d_{xy}$ ,  $d_{xz}$  and  $d_{yz}$  originated from crystal field splitted  $Ti:3d - t_{2g}$  orbitals located at the interface or in its vicinity.<sup>20</sup> Using combination of k.p envelope function method and density functional theory, Heering et al.<sup>21</sup> confirmed the existence of many anisotropic and non-parabolic sub-bands, which are only a few meV apart. Meanwhile, Zhong et al.<sup>6</sup> predicted a large spin-orbit splitting at the crossing point of the  $d_{xy}$  and  $d_{xz,yz}$  bands using density functional theory. To date, the predicted band-structure has received only partial support from transport experiments. Indeed, the analysis of Shubnikov-de Haas Oscillations (SdHO) provided distinctive results with respect to different experimental conditions and sample preparation methods. In refs,<sup>11,12</sup> the authors reported independently a single SdHO frequency and pointed out the possible valley and/or spin degeneracy of the electronic states to account for the discrepancy between the carrier density extracted from the SdHO and the Hall effect. Later, double SdHO frequencies perceived up to a moderate magnetic field (8 T) and at low temperature (50 mK)

were attributed to carriers populating the heavy sub-bands  $d_{xz}$  and  $d_{yz}$  splitted by the Rashba spin-orbit interaction.<sup>22</sup> On the other hand, McCollam et al.<sup>13</sup> extracted four frequencies using high magnetic field (20 T) for the SrTiO<sub>3</sub>/SrCuO<sub>3</sub>/LaAlO<sub>3</sub>/SrTiO<sub>3</sub> hetero-structure, and assigned these frequencies to four sub-bands of different mobilities. In contrast, very high field (55 T) measurements reveal quasi- $1/B$  periodic oscillations with an apparent single frequency, which emphasizes the role of Rashba spin-orbit interaction.<sup>14</sup> No consensus is reached in the interpretation of the magneto-transport properties and further work is needed to enrich the debate. In addition, it is worth mentioning that a systematic discrepancy between the carrier density estimated from Hall effect ( $n_{Hall}$ ) and SdHO ( $n_{SdHO}$ ) is reported by several groups.<sup>11,12,14</sup>

Here, we investigate the transport properties of a high mobility ( $\mu > 10^4 \text{ cm}^2 \text{ V}^{-1} \text{ s}^{-1}$ ) 2DEG at the LAO/STO interface under very high magnetic field (55 T) and low temperature (1.6 K). We observe strong  $1/B$ -aperiodic SdHO where the frequency increases with magnetic field. The hypotheses leading to this unexpected effect are discussed below, after reviewing the experimental data.

## RESULTS

The sample under investigation consists of 8 unit cells of LAO grown on top of a 500  $\mu\text{m}$  STO (001) substrate using a pulsed laser deposition technique at the temperature of 760 °C and in  $2 \times 10^{-6}$  Torr oxygen pressure. After the LAO growth, the sample is annealed in  $6 \times 10^{-2}$  Torr oxygen pressure at a temperature of 600 °C to remove oxygen vacancies. High Resolution Scanning Transmission Electron Microscope (HRSTEM) analysis reveals a mono-crystalline LAO layer without surface roughness while a large cation intermixing extends within two-three unit cells from the interface in both LAO and STO. The lattice spacing is expanded of about 5.5% along the growth axis, however no distortion is

<sup>1</sup>Laboratoire National des Champs Magnétiques Intenses (LNCMI-EMFL), Université de Toulouse, CNRS, INSA, UPS, 143 Avenue de Rangueil, 31400 Toulouse, France. <sup>2</sup>CEMES, Université de Toulouse, CNRS, UPS, 29 rue Jeanne-Marvig, F-31055 Toulouse, France. <sup>3</sup>Department of Physics and NUSNNI-Nanocore, National University of Singapore, 117411 Singapore, Singapore; <sup>4</sup>Present address: High Field Magnet Laboratory (HFML-EFML), Radboud University, 6525 ED Nijmegen, The Netherlands. \*email: rubi.km@lncmi.cnrs.fr; phyarian@nus.edu.sg

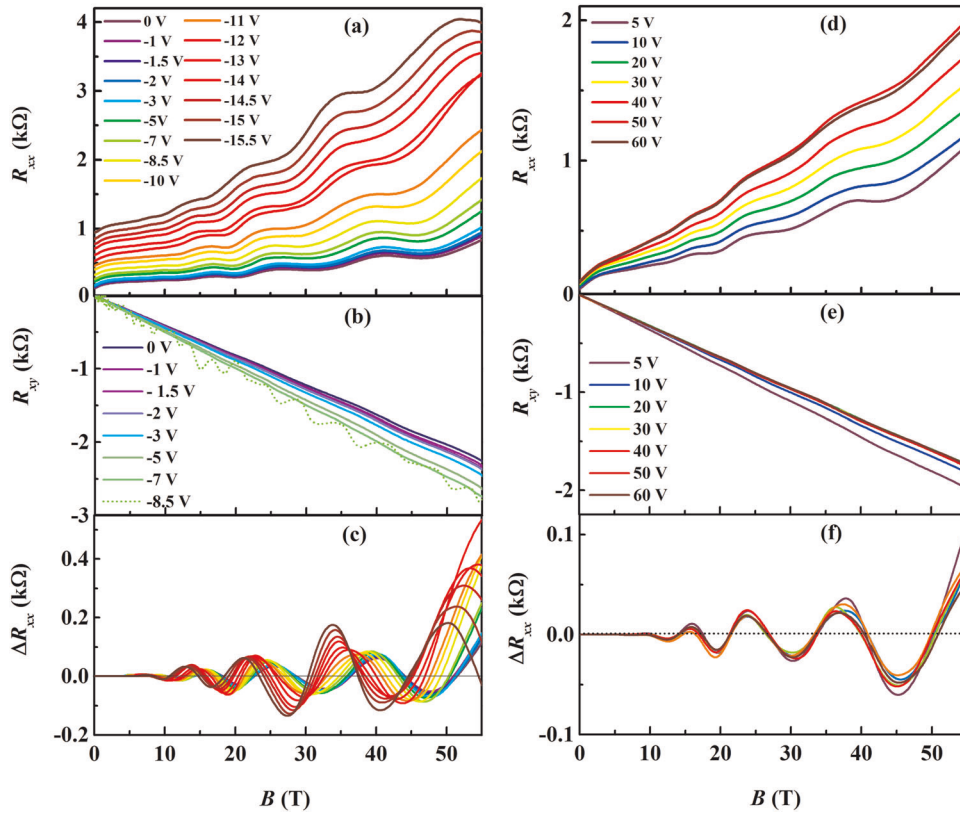


**Fig. 1** Left panels: magnetic field dependence of (a)  $R_{xx}$ , (b)  $R_{xy}$  and (c)  $\Delta R_{xx}$  for different values of  $V_g$  in the range  $0 \rightarrow -15.5$  V. Right panels: magnetic field dependence of (d)  $R_{xx}$ , (e)  $R_{xy}$  and (f)  $\Delta R_{xx}$  for different values of  $V_g$  in the range  $5 \rightarrow +60$  V. The temperature is 1.6 K.  $\Delta R_{xx}$  is the oscillating part of  $R_{xx}$  after extracting the monotonous background. A significant back-gate induced shift in the position of the  $\Delta R_{xx}$  oscillations extrema is observed only for  $V_g < 5$  V. Above this value, the oscillation pattern is almost unchanged concurrent with the saturation of  $n_{\text{Hall}}(V_g)$ .

observed in the growth plane. The sample is tailored into a Hall bar of width  $50 \mu\text{m}$  and length  $160 \mu\text{m}$  (see Supplementary information 1). Both the longitudinal magneto-resistance ( $R_{xx}$ ) and the Hall resistance ( $R_{xy}$ ) are measured simultaneously during a pulse of magnetic field up to 55 T at a temperature  $T = 1.6$  K. Such measurements are repeated for several values of back-gate voltage  $V_g$ , which is applied at the rear face of the STO substrate to modulate the carrier density of the 2DEG. The panels a and b of Fig. 1 show the magnetic field dependence of  $R_{xx}$  and  $R_{xy}$ , respectively, recorded at different back-gate voltages from 0 to  $-15.5$  V. The depopulation of the 2DEG leads to a substantial increase in zero-field resistance as well as an increasing positive magneto-resistance. In contrast, the longitudinal and Hall resistances change marginally as the back-gate voltage is set at positive values in the range  $\sim 5$ – $60$  V as shown in Fig. 1d, e. After subtracting the monotonic background (see Supplementary Information 2), we show  $\Delta R_{xx}(B) = R_{xx}(B) - \langle R_{xx}(B) \rangle$  for various  $V_g$  in Fig (c) and (f), respectively. While the position of the extrema in  $\Delta R_{xx}(B)$  spectra shifts significantly towards a lower magnetic field for negative back-gate voltages, a slight deviation is noticed above  $V_g \sim 5$  V, which reflects a saturation of the carrier density.

The Hall carrier concentration ( $n_{\text{Hall}}$ ) estimated from the slope of the linear fit of  $R_{xy}(B)$  and mobility ( $\mu_{\text{Hall}}$ ) are plotted versus  $V_g$  in Fig. 2. Taking into account the electric field dependence of the STO dielectric constant<sup>23</sup> the plane capacitor model (Supplementary Information 3) reproduces well the experimental Hall carrier density in the back-gate voltage range  $-7 \text{ V} < V_g < 5$  V. For negative back-gate voltages, the mobility decreases due to the enhanced electron's sensitiveness to emerging local potential fluctuations. Indeed, as the carrier density becomes low, screening of charged defects in the close environment of the 2DEG vanishes,

leading to a rise of the scattering rate. For  $V_g < -7$  V, the Hall voltage shows large temporal fluctuations and eventually becomes unmeasurable (see dotted-lines in Fig. 1(b)), as if the sample was turned into an insulator. This reversible trend is confirmed by  $R_{xx}$  which abruptly exceeds the measurement limit ( $\sim 1$  M $\Omega$ ) for  $V_g < -15.5$  V. In this regime, i.e., when the Hall 2DEG carrier density is below the threshold value of  $\sim 0.98 \times 10^{13} \text{ cm}^{-2}$ , electron localization arises successively in different locations of the sample, leading to a transport regime governed by the presence of percolating conduction paths. This scenario, in agreement with the direct visualization of sub-micrometer electron puddles using scanning SQUID spectroscopy<sup>24</sup> and inter-modulation electrostatic force microscopy,<sup>25</sup> provides a natural explanation for the apparent mismatch between  $R_{xx}$  and  $R_{xy}$  back-gating insulating thresholds. On the other hand, when the back-gate voltage is pushed beyond  $+10$  V, the Hall carrier density saturates to a maximum value of  $\sim 1.95 \times 10^{13} \text{ cm}^{-2}$ . This response is accompanied by a strong hysteretic behavior, which originates from the trapping of electrons by defects.<sup>26,27</sup> Indeed, assuming that the 2DEG is confined in a potential well close to the interface with the Fermi energy lying close to the top of the well, a positive back-gate voltage modifies the well profile and bends the STO conduction band. As a consequence, electrons can irreversibly escape the well and get trapped by defects. Interestingly, the carrier density can be reset to its  $V_g = 0$  V initial value (after a round trip to  $+60$  V at 1.6 K) by warming up the sample slightly above 20 K. We thus infer a very small average trapping energy of the order of 2 meV in our sample. We conjecture that the growing number of ionized defects, acting as remote scattering centers, is responsible for the variation of the Hall mobility which decreases simultaneously with the onset of carrier density saturation.

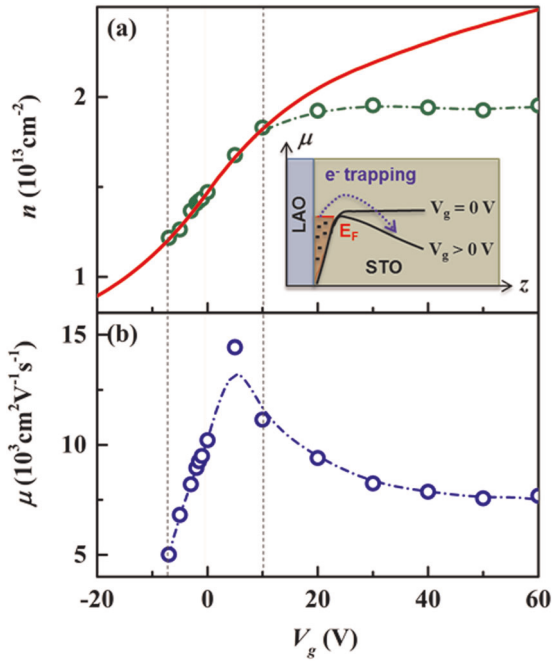


**Fig. 2** **a** Charge carrier density estimated from the Hall resistance (green symbols) and the plane capacitance model (red solid line). **b** Electron mobility estimated from the Hall density and the zero-field longitudinal resistance. The dash lines are guides for the eyes. The region between two vertical dotted lines ( $-7 \text{ V} < V_g < 10 \text{ V}$ ) indicates a reversible back-gate induced electron density modulation. The right side of the vertical line represents an hysteretic charge trapping/detrapping regime by ionized defects, leading to a saturation of the carrier density. The inset depicts an illustration of the LAO/STO interface including confining potential and electron trapping process.

Oxygen vacancies are often cited as potential defects in oxides but, even though investigations on the nature of the defects is certainly beyond the scope of this study, we believe that they are not at play in the electron trapping process. Indeed, first we remind that our sample was annealed in oxygen atmosphere and the resulting carrier density is lower than that typically obtained from the LAO/STO interfaces prepared in a low oxygen partial pressure without a subsequent high pressure post-annealing. Second, the oxygen vacancies are positively charged when they transfer one or two electrons to the 2DEG. The capture of electrons with increasing back-gate voltage would render them neutral, which is inconsistent with the experimentally observed mobility decrease. The main panel of Fig. 3a focuses on the inverse magnetic field dependence  $\Delta R_{xx}$  for  $V_g = 0 \text{ V}$ . We notice that the frequency of the oscillations increases monotonically with increasing magnetic field in our LAO/STO sample. This unexpected effect becomes clearer in the Landau plot, where the extrema of the oscillations are plotted as a function of  $1/B$  in the inset of Fig. 3a. Interestingly, the Landau plot is highly nonlinear, contrary to the standard 2DEG in semiconductor heterostructures or in graphene. As a matter of fact, the SdHO aperiodicity was apparent in the early literature of quantum transport in LAO/STO systems above 1 K.<sup>11,28</sup> However, this evidence has probably been overlooked due to the narrow magnetic field range and limited number of oscillations. Similarly,  $\delta$ -doped STO also exhibits aperiodic oscillations up to  $B_{\text{max}} = 15 \text{ T}$  in reference.<sup>29</sup> Our magneto-resistance data could certainly be fitted using an appropriate combination of  $1/B$ -periodic signals, referring to a complex set of unresolved sub-bands in the experimental conditions of temperature, magnetic field and samples' mobility. Although this multi-band model cannot be a priori discarded, the

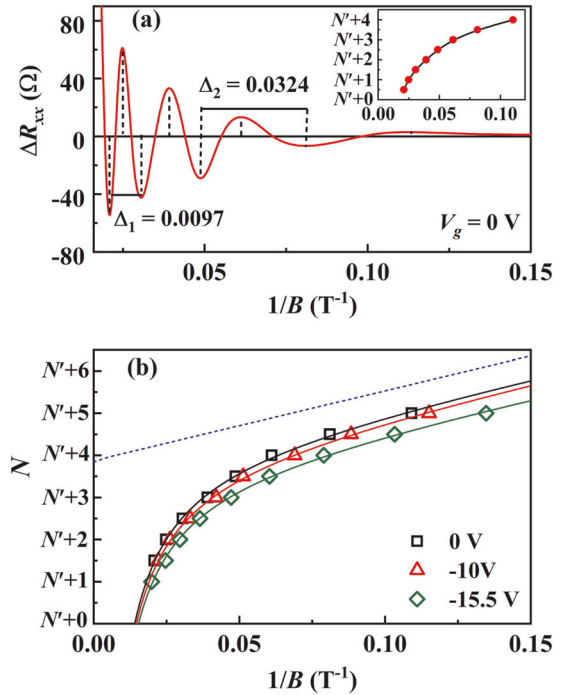


**Fig. 3** **a** Main panel: Inverse field dependence of  $\Delta R_{xx}$  for  $V_g = 0 \text{ V}$ . Inset: the corresponding Landau plot. Maxima and minima of  $\Delta R_{xx}(1/B)$  are assigned to integer and half-integer indices, respectively. **b** Landau level plots (symbols) for  $V_g = 0 \text{ V}$ ,  $-10$  and  $-15.5 \text{ V}$  fitted with Eq. (3) (solid lines). The dash line represents the asymptote for  $V_g = 0 \text{ V}$  derived from the fitting parameters  $F_{(\mu,0)}$  and  $\gamma_{(\mu,0)}$ —See also Table 1. The index  $N$  is given within an integer offset ( $N'$ ).

smooth evolution of the oscillating features call for alternative interpretations. In the following, we discuss different possible scenarios that can lead to the  $1/B$ -aperiodic SdHO, while keeping in mind that due to the limited number and the poor low-field resolution of the observed oscillations, the apparent  $1/B$ -aperiodicity may or may not have an intrinsic origin.

## DISCUSSION

When plotted as a function of inverse magnetic field, the frequency  $F = \frac{hS}{(2\pi)^2 e}$  of the magneto-resistance oscillations is proportional to the area in the reciprocal space of the cyclotron orbit  $S$ , which obeys the Onsager's quantization condition:

$$S = \frac{(2\pi)^2 eB}{h} \times \left( N + \frac{1}{2} \right) \quad (1)$$

Here  $h$  and  $e$  are respectively the Planck constant and the electron charge, and  $N$  is a positive integer index related to the formation of Landau levels.  $S$  is linked to the carrier density  $n_{\text{SdH}}$  and to the topology of the Fermi surface. Taking into account the total degeneracy ( $g = g_s g_v$ ) of the quantum states, these parameters set the Fermi energy  $E_F$  (e.g., the chemical potential  $\mu$ , assuming low enough temperature). To explain the continuous increase of the frequency  $F$  as the magnetic field rises, we are left to question (i) the quantization rule itself as well as the possible magnetic field dependence of (ii)  $E_F$  and (iii)  $n_{\text{SdH}}$ .

The scenario (i) is met when the quantization of the electron's kinetic energy results from a competition between the electrical and the magnetic confinement. This route has been recently explored by G. Cheng et al.<sup>30</sup> who studied the conductance of an individual and artificially designed quasi-1D conduction channel at the LAO/STO interface. The model, derived from,<sup>31</sup> predicts an

**Table 1.** Parameters determined from the fit of the Landau plot.

References	$F_{(\mu, 0)}$	$-\gamma_{(\mu, 0)}$	$C_{(\mu, 0)}$	$n_{\text{Hall}} \text{ (cm}^{-2}\text{)}$	$n_{\text{SdH}} \text{ (cm}^{-2}\text{)}$
This work ( $V_g = 0 \text{ V}$ )	16.56	$N' + 3.87$	−0.057	$1.47 \times 10^{13}$	$8.02 \times 10^{11}$
This work ( $V_g = -10 \text{ V}$ )	15.74	$N' + 3.76$	−0.058	$1.12 \times 10^{13}$	$7.62 \times 10^{11}$
This work ( $V_g = -15.5 \text{ V}$ )	11.68	$N' + 3.61$	−0.062	$0.98 \times 10^{13}$	$5.66 \times 10^{11}$
<sup>11</sup>	14.49	$N' + 3.62$	−0.19	$1.05 \times 10^{13}$	$6.96 \times 10^{11}$
<sup>28</sup>	8.94	$N' + 3.68$	−0.24	$0.56 \times 10^{13}$	$4.28 \times 10^{11}$

The phase  $\gamma_{(\mu, 0)}$  is given to within an integer offset  $N'$ . The Hall carrier density  $n_{\text{Hall}}$  for  $V_g = -10 \text{ V}$  and  $-15.5 \text{ V}$  is taken from the extrapolated plane capacitor model fitting in Fig. 2a.

alteration of the oscillations' frequency which can merely fit our experimental data (see Supplementary Information 4). However, this approach must be adapted to the quasi-2D nature of our sample by considering the presence of an incoherent network of quasi-1D channels at the interface. Even if this hypothesis may find an echo with the formation of percolation paths at low carrier density, or with the presence of grain boundaries acting as potential wells, the origin of the quasi-1D channels remain strongly elusive.

The hypothesis (ii) refers to a magnetic field-induced change of the Fermi surface topology, while the carrier density is kept constant. In this scenario, the chemical potential of the system is allowed to change as the magnetic field affects the electron's dynamics. In pure 2D systems, a constant carrier density necessarily implies a fixed frequency for the Shubnikov-de Haas oscillations, regardless any eventual variation of the chemical potential or Fermi surface topology. This is because the kinetic energy of the electrons is affected by the (perpendicular) magnetic field and must fit into Landau levels. Therefore, the  $1/B$ -periodic magnetic oscillations results from the filling of a fixed number of electrons into Landau levels, whose degeneracy is strictly proportional to the magnetic field. This picture, however, no longer holds if one introduces other energy scales due to spin-orbit coupling, Zeeman effect and disorder. Indeed, the Landau level energy ladder can be strongly modified, ensuing the formation of new energy levels with different effective degeneracy.<sup>14,22</sup> In particular, Trier et al.<sup>28</sup> pointed out a Zeeman energy  $g\mu_B \cdot B$  comparable to the orbital Landau level gap  $\hbar eB/m^*$  for large effective mass ( $m^* \sim 1.3 \times m_e$ ) in LAO/STO. This model predicts an unusual magnetic field doubling of the oscillation's frequency corresponding to the transition from a spin-degenerate to a spin-resolved Landau level ladder. We note, however, that the Zeeman effect alone cannot explain our experimental results since the frequency of the oscillations is actually multiplied by 3.6 (e.g., larger than 2) from 12 to 34 T. Rashba spin-orbit coupling certainly affects the topology of the Fermi surface and consequently the periodicity of the quantum oscillations. Based on the work of Fete et al.,<sup>22</sup> Yang et al.<sup>14</sup> have discussed this scenario to explain the quasi  $1/B$ -periodic nature of the oscillations in the same system. However, we could not fit our present data (with larger aperiodicity) using this model. We note that the Rashba effect is certainly oversimplified in this model, and a more accurate description requires advanced and dedicated calculations which are out of the scope of the present manuscript. In contrast, deviations from strictly  $1/B$ -periodic oscillations are well known in 3D systems for small Landau level indices.<sup>32</sup> This effect is however too weak to compare with our experimental observations, provided the electron gas at the LAO/STO interface can be regarded as a (quasi)-3D system. In the context of a fixed number of electrons, a deformation (reconstruction) of the Fermi surface, eventually driven by the Coulomb interaction, is likely to trigger a field-induced Lifshitz transition. However, we expect this phenomenon to translate into a sharp signature in the magneto-resistance

at a certain value of the magnetic field in contrast with the smooth evolution of the oscillation's frequency and amplitude.

The assumption (iii) considers the case of a variable carrier density while the chemical potential is kept constant. Similar to graphene on silicon carbide,<sup>33,34</sup> one possibility is to infer that electrons are continuously transferred from a nearby reservoir to the LAO/STO interface as the magnetic field increases. Although this model sounds attractive, it relies on a hypothetical charge reservoir with strong capacitive coupling to the 2DEG, so that the quantum capacitance of the system drives the charges' dynamics. To our knowledge, we are not aware of any charge reservoir in the vicinity of the LAO/STO interface and this hypothesis is therefore discarded. On the other hand, inspired by the recent work of Gao and Niu,<sup>35</sup> who introduced a generalized Onsager's relation to explain the  $1/B$ -aperiodic quantum oscillations observed in systems with complex topological order, we now consider an alternative approach involving the magnetic response functions of the system. Following the lines of Fuchs et al.,<sup>36</sup> the averaged carrier density  $\langle n \rangle$  derives from the derivative of the grand potential  $\Omega_{(\mu, B)}$  with respect to the chemical potential  $\mu$ , which is itself expanded in Taylor series with respect to the magnetic field:

$$\langle n \rangle = -\frac{1}{S} \frac{\partial}{\partial \mu} (\Omega_{(\mu, B)}) = -\frac{\partial}{\partial \mu} \left( \frac{1}{S} \Omega_{(\mu, 0)} - m_0 \times B - \frac{\chi_0}{2} \times B^2 + \dots \right) \quad (2)$$

where  $m_0 = -\frac{1}{S} \frac{\partial}{\partial B} (\Omega_{(\mu, 0)})$  and  $\chi_0 = -\frac{1}{S} \frac{\partial^2}{\partial B^2} (\Omega_{(\mu, 0)})$  are the averaged magnetization and magnetic susceptibility at zero field, respectively. Combining Eqs. (2) and (1) and setting  $n_0 \equiv -\frac{1}{S} \frac{\partial}{\partial \mu} (\Omega_{(\mu, 0)})$  one obtains:

$$N = F_{(\mu, 0)} \times \frac{1}{B} - \gamma_{(\mu, 0)} + C_{(\mu, 0)} \times B + \dots \quad (3)$$

where  $F_{(\mu, 0)}$  is the frequency of the oscillations at low magnetic field, e.g., the slope of the Landau diagram asymptote for  $1/B \rightarrow \infty$ . The coefficient  $\gamma_{(\mu, 0)} = \frac{1}{2} - \frac{\partial m_0}{\partial \mu}$  sets the phase of the Shubnikov-de Haas oscillations and corresponds to the intercept of asymptote for  $1/B \rightarrow \infty$  with the index axis in the Landau plot. Finally, the coefficient  $C_{(\mu, 0)} = \frac{\hbar}{4 \cdot e} \frac{\partial \chi_0}{\partial \mu}$  is linked to the curvature of the Landau plot. Table 1 reports the best fitting parameters  $F_{(\mu, 0)}$ ,  $\gamma_{(\mu, 0)}$  and  $C_{(\mu, 0)}$  determined from the fit of the experimental data (this work and literature—Supplementary Information 5) to Eq. 3, as well as the Hall carrier density ( $n_{\text{Hall}}$ ) and the SdHO carrier density ( $n_{\text{SdH}} = \frac{2 \cdot e}{h} F_{(\mu, 0)}$ ) for comparison.

Interestingly, all the parameters exhibit a monotonous evolution with gate voltage (see Supplementary Information 6). While  $F_{(\mu, 0)}$  and  $\gamma_{(\mu, 0)}$  from high (55 T—this work) and low field (12 T—refs <sup>11,28</sup>) experimental data are of the same order of magnitude, a fair discrepancy occurs in  $C_{(\mu, 0)}$  for different field regimes and carrier density. The variance of  $C_{(\mu, 0)}$  can be explained by (i) different carrier density, (ii) different levels of disorder, and (iii) magnetic field range over which the fit is performed. It is actually worth mentioning that the accuracy of the fit parameters is restricted by the limited number of oscillations,

especially at low field. Even if the recent observation of non-zero magnetic response functions<sup>3,9,37</sup> of the LAO/STO interface and the expected enhanced susceptibility in the low-electron-density regime<sup>38</sup> are in line with the non-linear Landau plots, improved precision on  $\gamma_0(E)$  and  $C(E)$  is needed in order to obtain a quantitative agreement.

The cases (ii) and (iii) are certainly an idealization of real systems, where both the charge carrier concentration and the chemical potential may indistinguishably vary. The combined effects translate into a change of  $S$  as a function of the magnetic field, whose relative increase reaches up to 1000% in the 0–55 T magnetic field range, assuming a zero-field electron density of  $1 \times 10^{12} \text{ cm}^{-2}$  (See Supplementary Information 7). At first sight, the linear Hall effect tends to favor a scenario with a constant carrier density. However, this claim must be taken with care since a quasi-linear Hall effect is allowed in a multi-carrier system with fixed total charge density. A magnetic field-induced transfer of electrons from low-mobility to high-mobility bands is indeed compatible with an increase of the quantum oscillations' frequency, while the Hall coefficient is only weakly affected. It is worth to mention that the non-trivial band-structure of the LAO/STO interface at the Fermi energy may also generate aperiodic oscillations in high field regime similar to the non-ideal Dirac fermion systems.<sup>39</sup>

The hypothesis (iii) provides a new approach to compute the carrier density from aperiodic oscillations which was otherwise systematically over-estimated using fast Fourier transform (FFT) analysis. Indeed, the strong aperiodicity tends to broaden the FFT spectrum towards high frequency and can even favor the onset of spurious FFT peaks when the magnetic field range is extended towards very high magnetic field (see Supplementary Information 8). To complement this insight, we revisit the large discrepancy between  $n_{\text{Hall}}$  and  $n_{\text{SdHO}}$  using density functional theory (DFT) calculations, where the density of states projection of the  $d_{xy}$  and  $d_{xz}/d_{yz}$  subbands at the Fermi energy is investigated. The layer-resolved density of states with electronic band structure of the LAO/STO interface are shown in Fig. 4. The lower lying  $d_{xy}$  subbands ( $1d_{xy}$  and  $2d_{xy}$ ) are populated by a majority of electrons located mainly into the first two  $\text{TiO}_2$  planes from the interface. On the other hand,  $d_{xz}/d_{yz}$  subbands are populated by a minority of electrons whose spatial extension expands from the second to the

sixth  $\text{TiO}_2$  plane. Based on HRSTEM analysis, we conjecture that cation intermixing, strain and probably the non-homogeneous valence of the titanium atoms generate potential fluctuations in the two first layers of STO at least, which strongly affect the electronic mobility. Therefore, the majority of electrons belonging to the  $1d_{xy}$  and  $2d_{xy}$  subbands will have low mobility even if they display low effective mass and do not engender quantum oscillations. They contribute mainly to the linear Hall effect with a theoretical carrier density estimated to  $n_{d_{xy}} \approx 6 \times 10^{13} \text{ cm}^{-2}$ . The SdHO ensue from the minority charge carriers located deeper in STO and belonging to the higher energy  $d_{xz}/d_{yz}$  subbands. The cyclotron mass,  $m_c = 1.75 + 0.05m_e$  estimated from the Lifshitz-Kosevich equation fitting (see Supplementary Information 9) is consistent with the theoretically calculated averaged effective mass ( $m^* \sim 1.8m_e$ ) of the  $d_{xz}/d_{yz}$  subbands. The theoretical carrier density for these subbands is estimated to  $n_{d_{xz}/d_{yz}} \approx 5.2 \times 10^{12} \text{ cm}^{-2}$  taking into account the fourth, fifth, and sixth layers where the density of state projection of the  $d_{xz}/d_{yz}$  subbands is relevant. Even if the DFT based model does not reflect a realistic LAO/STO system (for instance the presence of defects is not taken into account and the exact position of the Fermi energy is unknown), this study shows that a large ratio of  $n_{\text{Hall}}$  and  $n_{\text{SdHO}}$  ( $n_{\text{Hall}}/n_{\text{SdHO}} \sim 13 - 18$  from Table 1) observed experimentally can be conveniently explained by the relative population of the  $d_{xy}$ ,  $d_{xz}$  and  $d_{yz}$  subbands, where  $n_{d_{xy}/d_{xz}/d_{yz}}/n_{d_{xz}/d_{yz}}$  approaches  $\sim 14$ .

The magneto-transport properties of a high-mobility electron gas at the LAO/STO interface are studied under high magnetic field (55 T) and low temperature (1.6 K) for different carrier densities. We observe  $1/B$ -aperiodic SdHO over the full magnetic field range (9–55 T). The aperiodic character of the oscillations involves the failure of standard FFT data processing, unless the analysis is restricted to low enough magnetic field. Pre-empting the fact that only very low temperature combined with high-field measurements are necessary to address the extrinsic (multi-band) origin of the measured  $1/B$ -aperiodic oscillations, we explore several alternative scenarios which provide new insights and bring further evidence for a non-trivial band structure at the Fermi energy, in consistency with DFT calculations where  $d_{xy}$ ,  $d_{xz}$  and  $d_{yz}$  subband anti-crossings occur due to spin-orbit coupling. When the Fermi energy is located in the vicinity of the  $d_{xz}/d_{yz}$  subbands bottom, a fair correspondence can be established between electrons' location within the  $\text{TiO}_2$  planes and the subbands

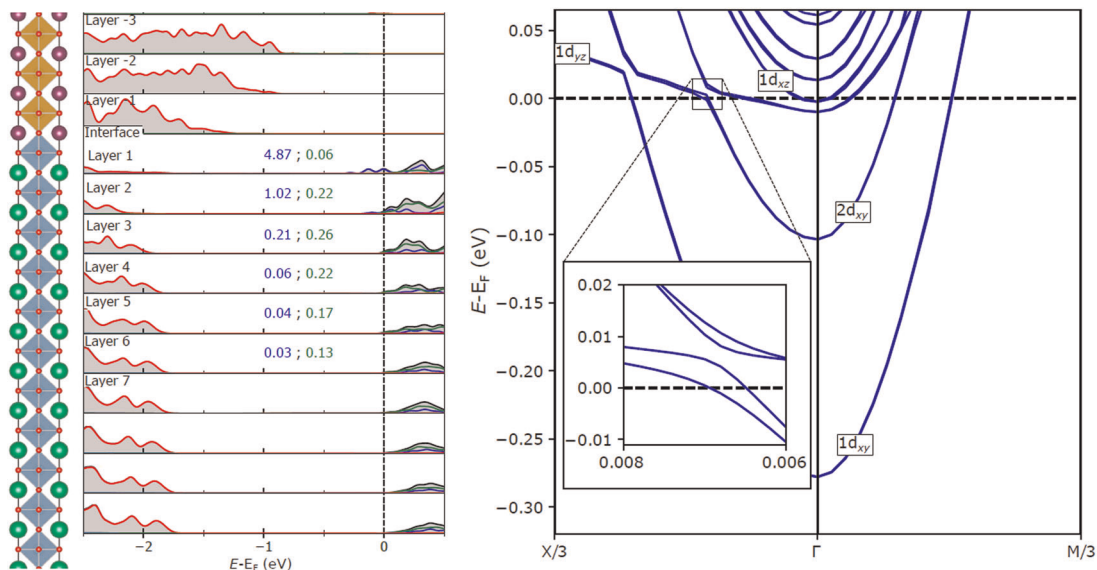


**Fig. 4** Left panel: The layer-resolved density of states (LDOS) in LAO/STO. Each LDOS corresponds to a  $\text{AlO}_2$  or  $\text{TiO}_2$  plane. The black curve corresponds to the total LDOS of the  $\text{TiO}_2$  plane, the blue, green and red curves correspond respectively to the  $d_{xy}$  orbital, the  $d_{yz} + d_{xz}$  orbitals of Ti and the 2p states of oxygen. Right panel: Electronic band structure of the STO in LAO/STO system. Inset shows a zoomed-in view of band avoiding and splitting due to the atomic and Rashba spin-orbit coupling.

to whom they belong. The majority electrons populating the  $d_{xy}$  subbands are located close to the interface and are sensitive to interface disorder as revealed by HRSTEM analysis. Their low mobility and high carrier density explain the linear field dependence of the Hall resistance. On the other hand, the minority of charge carriers belonging to the  $d_{xz}/d_{yz}$  bands and located deeper from the interface are responsible for the SdHO with strong aperiodic behavior. In this scheme, the long-standing issue regarding the mismatch in carrier density extracted from the Hall effect and the SdHO finds a qualitative explanation, based on the sample's dependent relative population of the  $d_{xz}$ ,  $d_{yz}$  and  $d_{xy}$  subbands.

## METHODS

### Sample fabrication and structural characterization

The 8 unit cells of LaAlO<sub>3</sub> film were grown on a TiO<sub>2</sub>-terminated (001) SrTiO<sub>3</sub> single crystal using pulse laser deposition (PLD) technique at NUSNNI-Nanocore National University of Singapore (NUS). The Lambda Physik Excimer KrF UV laser with the wavelength of 248 nm at a pulse rate of 1 Hz was used in PLD. The layer-by-layer growth of LaAlO<sub>3</sub> was precisely controlled by in situ reflection high energy electron diffraction (RHEED). During growth, the oxygen partial pressure  $P_{(O_2)}$  and temperature were maintained at  $2 \times 10^{-6}$  torr and 760 °C, respectively. After growth, the sample was cooled down to room temperature at a rate of 5 °C/min with same  $P_{(O_2)}$ . Later, the sample was annealed in the  $P_{(O_2)}$  of 60 mtorr and at the temperature of 600 °C. The six-terminal Hall bar device of width 50 μm and length 160 μm between the longitudinal voltage leads was fabricated by conventional photolithography technique using AlN films as hard mask. The optical microscopy image of the Hall bar device is shown in the Supplementary Information 1. The cross-section of the LAO/STO structure was characterized using a probe Cs-corrected JEOL JEM-ARM200F Transmission Electron Microscope (TEM) operated at 200 kV at CEMES. Focused ion beam was used to prepare the TEM lamella.

### Transport measurements

The transport measurements under high magnetic field and low temperatures were carried out at Laboratoire National des Champs Magnétiques Intenses (LNCMI) Toulouse. For transport measurements, the device was electrically bonded with Al wires using wedge bonding. The sample was cooled down from room temperature to 1.6 K with a cooling rate of ~3 K/min in a He4 cryostat. The sheet resistance decreases from 250 kΩ to 130 Ω as the temperature is decreased from 300 K to 1.6 K. The simultaneous measurements of longitudinal and Hall voltages were performed under high pulsed magnetic field of up to 55 T with duration 300 ms and at  $T = 1.6$  K. The back-gate voltage was varied from 0 to -15.5 V and from 0 to 60 V for tuning the carrier density at the interface. The dc current excitation was 1 μA. All magneto-transport measurements were performed with the magnetic field oriented perpendicular to the sample's plane.

### First-principles calculations

The ab initio calculations have been performed using the plane wave code VASP<sup>40,41</sup> and the generalized gradient approximation (GGA)<sup>42</sup> for the exchange-correlation energy. More details are given in the Supplementary Information 10.

## DATA AVAILABILITY

The data generated and/or analyzed in this study are available from the corresponding author upon reasonable request.

Received: 23 September 2019; Accepted: 30 December 2019;

Published online: 30 January 2020

## REFERENCES

- Ohtomo, A. & Hwang, H. A high-mobility electron gas at the LaAlO<sub>3</sub>/SrTiO<sub>3</sub> heterointerface. *Nature* **427**, 423–426 (2004).
- Reyren, N. et al. Superconducting interfaces between insulating oxides. *Science* **317**, 1196–1199 (2007).
- Li, L., Richter, C., Mannhart, J. & Ashoori, R. C. Coexistence of magnetic order and two-dimensional superconductivity at LaAlO<sub>3</sub>/SrTiO<sub>3</sub> interfaces. *Nat. Phys.* **7**, 762–766 (2011).
- Stornaiuolo, D. et al. Signatures of unconventional superconductivity in the LaAlO<sub>3</sub>/SrTiO<sub>3</sub> two-dimensional system. *Phys. Rev. B* **95**, 140502 (2017).
- Ben Shalom, M., Sachs, M., Rakhmilevitch, D., Palevski, A. & Dagan, Y. Tuning spin-orbit coupling and superconductivity at the LaAlO<sub>3</sub>/SrTiO<sub>3</sub> interface: a magnetotransport study. *Phys. Rev. Lett.* **104**, 126802 (2010).
- Zhong, Z., Tóth, A. & Held, K. Theory of spin-orbit coupling at LaAlO<sub>3</sub>/SrTiO<sub>3</sub> interfaces and SrTiO<sub>3</sub> surfaces. *Phys. Rev. B* **87**, 161102 (2013).
- Caviglia, A. D. et al. Tunable Rashba spin-orbit interaction at oxide interfaces. *Phys. Rev. Lett.* **104**, 126803 (2010).
- Brinkman, A. et al. Magnetic effects at the interface between non-magnetic oxides. *Nat. Mater.* **6**, 493–496 (2007).
- Bert, J. A. et al. Direct imaging of the coexistence of ferromagnetism and superconductivity at the LaAlO<sub>3</sub>/SrTiO<sub>3</sub> interface. *Nat. Phys.* **7**, 767–771 (2011).
- Ariando, A. et al. Electronic phase separation at the LaAlO<sub>3</sub>/SrTiO<sub>3</sub> interface. *Nat. Commun.* **2**, 188 (2011).
- Caviglia, A. D. et al. Two-dimensional quantum oscillations of the conductance at LaAlO<sub>3</sub>/SrTiO<sub>3</sub> interfaces. *Phys. Rev. Lett.* **105**, 236802 (2010).
- Ben Shalom, M., Ron, A., Palevski, A. & Dagan, Y. Shubnikov-de Haas oscillations in SrTiO<sub>3</sub>/LaAlO<sub>3</sub> interface. *Phys. Rev. Lett.* **105**, 206401 (2010).
- McCollam, A. et al. Quantum oscillations and subband properties of the two-dimensional electron gas at the LaAlO<sub>3</sub>/SrTiO<sub>3</sub> interface. *APL Mater.* **2**, 022102 (2014).
- Yang, M. et al. High field magneto-transport in two-dimensional electron gas LaAlO<sub>3</sub>/SrTiO<sub>3</sub>. *Appl. Phys. Lett.* **109**, 122106 (2016).
- Salluzzo, M. et al. Orbital reconstruction and the two-dimensional electron gas at the LaAlO<sub>3</sub>/SrTiO<sub>3</sub> interface. *Phys. Rev. Lett.* **102**, 166804 (2009).
- Reinle-Schmitt, M. et al. Tunable conductivity threshold at polar oxide interfaces. *Nat. Commun.* **3**, 932 (2012).
- Kalabukhov, A. et al. Effect of oxygen vacancies in the SrTiO<sub>3</sub> substrate on the electrical properties of the LaAlO<sub>3</sub>/SrTiO<sub>3</sub> interface. *Phys. Rev. B* **75**, 121404 (2007).
- Herranz, G. et al. High mobility in LaAlO<sub>3</sub>/SrTiO<sub>3</sub> heterostructures: origin, dimensionality, and perspectives. *Phys. Rev. Lett.* **98**, 216803 (2007).
- Fongkaew, I., Limpijumng, S. & Lambrecht, W. R. L. Effects of structural relaxation, interdiffusion, and surface termination on two-dimensional electron gas formation at the LaAlO<sub>3</sub>/SrTiO<sub>3</sub> (001) interface. *Phys. Rev. B* **92**, 155416 (2015).
- Delugas, P. et al. Spontaneous 2-dimensional carrier confinement at the LaAlO<sub>3</sub>/SrTiO<sub>3</sub> interface. *Phys. Rev. Lett.* **106**, 166807 (2011).
- van Heeringen, L. W., de Wijs, G. A., McCollam, A., Maan, J. C. & Fasolino, A. kp subband structure of the LaAlO<sub>3</sub>/SrTiO<sub>3</sub> interface. *Phys. Rev. B* **88**, 205140 (2013).
- Fête, A. et al. Large modulation of the Shubnikov-de Haas oscillations by the Rashba interaction at the LaAlO<sub>3</sub>/SrTiO<sub>3</sub> interface. *New J. Phys.* **16**, 112002 (2014).
- Neville, R. C., Hoeneisen, B. & Mead, C. A. Permittivity of strontium titanate. *J. Appl. Phys.* **43**, 2124–2131 (1972).
- Kalisky, B. et al. Locally enhanced conductivity due to the tetragonal domain structure in LaAlO<sub>3</sub>/SrTiO<sub>3</sub> heterointerfaces. *Nat. Mater.* **12**, 1091–1095 (2013).
- Aurino, P. et al. Retention of electronic conductivity in LaAlO<sub>3</sub>/SrTiO<sub>3</sub> nanostructures using a SrCuO<sub>2</sub> capping layer. *Phys. Rev. Appl.* **6**, 024011 (2016).
- Yu, L. & Zunger, A. A polarity-induced defect mechanism for conductivity and magnetism at polar-nonpolar oxide interfaces. *Nat. Commun.* **5**, 5118 (2014).
- Biscaras, J. et al. Limit of the electrostatic doping in two-dimensional electron gases of LaXO<sub>3</sub> (X = Al, Ti)/SrTiO<sub>3</sub>. *Sci. Rep.* **4**, 6788 (2014).
- Trier, F. et al. Quantization of Hall resistance at the metallic interface between an oxide insulator and SrTiO<sub>3</sub>. *Phys. Rev. Lett.* **117**, 096804 (2016).
- Jalan, B., Stemmer, S., Mack, S. & Allen, S. J. Two-dimensional electron gas in δ-doped SrTiO<sub>3</sub>. *Phys. Rev. B* **82**, 081103 (2010).
- Cheng, G. et al. Shubnikov de Haas like quantum oscillations in artificial one-dimensional LaAlO<sub>3</sub>/SrTiO<sub>3</sub> electron channels. *Phys. Rev. Lett.* **120**, 076801 (2018).
- Beenakker, C. & van Houten, H. Quantum transport in semiconductor nanostructures. In *Semiconductor Heterostructures and Nanostructures*, vol. 44 of *Solid State Physics* (eds Ehrenreich, H. & Turnbull, D.) 1–228 (Academic Press, 1991).
- Argyres, P. N. & Adams, E. N. Longitudinal magnetoresistance in the quantum limit. *Phys. Rev.* **104**, 900–908 (1956).
- Janssen, T. J. B. M. et al. Anomalous strong pinning of the filling factor  $\nu = 2$  in epitaxial graphene. *Phys. Rev. B* **83**, 233402 (2011).
- Yang, M. et al. Puddle-induced resistance oscillations in the breakdown of the graphene quantum hall effect. *Phys. Rev. Lett.* **117**, 237702 (2016).
- Gao, Y. & Niu, Q. Zero-field magnetic response functions in Landau levels. *Proc. Natl Acad. Sci. USA* **114**, 7295–7300 (2017).
- Fuchs, J. N., Piéchon, F. & Montambaux, G. Landau levels, response functions and magnetic oscillations from a generalized Onsager relation. *SciPost Phys.* **4**, 024 (2018).

37. Lee, J.-S. et al. Titanium  $d_{xy}$  ferromagnetism at the  $\text{LaAlO}_3/\text{SrTiO}_3$  interface. *Nat. Mater.* **12**, 703–706 (2013).
38. Fischer, M. H., Raghu, S. & Kim, E.-A. Spin–orbit coupling in  $\text{LaAlO}_3/\text{SrTiO}_3$  interfaces: magnetism and orbital ordering. *New J. Phys.* **15**, 023022 (2013).
39. Taskin, A. A. & Ando, Y. Berry phase of nonideal dirac fermions in topological insulators. *Phys. Rev. B* **84**, 035301 (2011).
40. Kresse, G. & Hafner, J. Ab initio molecular-dynamics simulation of the liquid-metal-amorphous-semiconductor transition in germanium. *Phys. Rev. B* **49**, 14251–14269 (1994).
41. Kresse, G. & Furthmüller, J. Efficient iterative schemes for ab initio total-energy calculations using a plane-wave basis set. *Phys. Rev. B* **54**, 11169–11186 (1996).
42. Perdew, J. P., Burke, K. & Ernzerhof, M. Generalized gradient approximation made simple. *Phys. Rev. Lett.* **77**, 3865–3868 (1996).

## ACKNOWLEDGEMENTS

This study has been supported through the grant NEXT n°ANR-10-LABX-0037 in the framework of the “Programme des Investissements d’Avenir”. We acknowledge the support of the LNCMI-CNRS, member of the European Magnetic Field Laboratory (EMFL). The NUS authors acknowledge the support from the NUS Academic Research Fund (AcRF Tier 1 Grants No. R-144-000-364-112, No. R-144-000-391-114, and No. R-144-000-403-114) and the Singapore National Research Foundation (NRF) under the Competitive Research Programs (CRP Grant No. NRF-CRP15-2015-01). This work was granted access to the HPC resources of the CALMIP supercomputing center under the allocation p1229. We are grateful to U. Zeitler, M. O. Goerbig, J. N. Fuchs, F. Piechon, and D. K. Maude for very insightful discussions.

## AUTHOR CONTRIBUTIONS

K.H., S.Z. and Z. H. grew the samples. K.R. performed high field magneto-transport experiments. J.G. and R.A. performed theoretical calculations. R.S., B.W.-F. and E.S. carried out HRSTEM experiments. All authors analyzed the data and discussed the results. K.R. and W.E. wrote the manuscript with input from all authors.

## COMPETING INTERESTS

The authors declare no competing interests.

## ADDITIONAL INFORMATION

**Supplementary information** is available for this paper at <https://doi.org/10.1038/s41535-020-0210-z>.

**Correspondence** and requests for materials should be addressed to K.R. or Ariando

**Reprints and permission information** is available at <http://www.nature.com/reprints>

**Publisher’s note** Springer Nature remains neutral with regard to jurisdictional claims in published maps and institutional affiliations.



**Open Access** This article is licensed under a Creative Commons Attribution 4.0 International License, which permits use, sharing, adaptation, distribution and reproduction in any medium or format, as long as you give appropriate credit to the original author(s) and the source, provide a link to the Creative Commons license, and indicate if changes were made. The images or other third party material in this article are included in the article’s Creative Commons license, unless indicated otherwise in a credit line to the material. If material is not included in the article’s Creative Commons license and your intended use is not permitted by statutory regulation or exceeds the permitted use, you will need to obtain permission directly from the copyright holder. To view a copy of this license, visit <http://creativecommons.org/licenses/by/4.0/>.

© The Author(s) 2020